Experimental Eye Research 240 (2024) 109813

Contents lists available at ScienceDirect

Experimental Eye Research

journal homepage: www.elsevier.com/locate/yexer

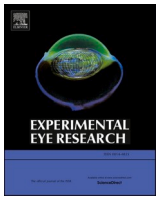

Research article

Lysyl oxidase like-1 deficiency in optic nerve head astrocytes elicits reactive astrocytosis and alters functional effects of astrocyte derived exosomes

Harsh N. Hariani [a,h], Anita K. Ghosh [a,h], Sasha M. Rosen [b,i], Huen-Yee Tso [g], Cassidy Kessinger [a], Chongyu Zhang [d], W. Keith Jones [c], Rebecca M. Sappington [e,f], Claire H. Mitchell [g], Evan B. Stubbs Jr. [b,h], Vidhya R. Rao [b,h], Simon Kaja [b,c,h,*]

[a] Graduate Program in Neuroscience, Loyola University Chicago, Maywood, IL, 60153, USA
[b] Department of Ophthalmology, Loyola University Chicago, Maywood, IL, 60153, USA
[c] Department of Molecular Pharmacology and Neuroscience, Loyola University Chicago, Maywood, IL, 60153, USA
[d] Graduate Program in Molecular Pharmacology and Therapeutics, Loyola University Chicago, Maywood, IL, 60153, USA
[e] Department of Biochemistry, Wake Forest University School of Medicine, Winston-Salem, NC, 27109, USA
[f] Translational Eye and Vision Research Center, Wake Forest University School of Medicine, Winston-Salem, NC, 27109, USA
[g] Basic and Translational Sciences, School of Dental Medicine, University of Pennsylvania, Philadelphia, PA, 19104, USA
[h] Research Service, Edward Hines Jr Veterans Affairs Hospital, Hines, IL, 60141, USA
[i] Department of Radiology, UC Davis Medical Center, Sacramento, CA, 95817, USA

ARTICLE INFO

Keywords:
Optic nerve head astrocytes
Reactive astrocytosis
Mechanical strain
Exosomes
Extracellular vesicles
Lysyl oxidase like 1
Elastin
Extracellular matrix

ABSTRACT

Glaucoma is a multifactorial progressive ocular pathology that manifests clinically with damage to the optic nerve (ON) and the retina, ultimately leading to blindness. The optic nerve head (ONH) shows the earliest signs of glaucoma pathology, and therefore, is an attractive target for drug discovery. The goal of this study was to elucidate the effects of reactive astrocytosis on the elastin metabolism pathway in primary rat optic nerve head astrocytes (ONHA), the primary glial cell type in the unmyelinated ONH. Following exposure to static equibiaxial mechanical strain, we observed prototypic molecular and biochemical signatures of reactive astrocytosis that were associated with a decrease in lysyl oxidase like 1 (*Loxl1*) expression and a concomitant decrease in elastin (*Eln*) gene expression. We subsequently investigated the role of Loxl1 in reactive astrocytosis by generating primary rat ONHA cultures with ~50% decreased Loxl1 expression. Our results suggest that reduced Loxl1 expression is sufficient to elicit molecular signatures of elastinopathy in ONHA. Astrocyte derived exosomes (ADE) significantly increased the length of primary neurites of primary neurons *in vitro*. In contrast, ADE from Loxl1-deficient ONHA were deficient of trophic effects on neurite outgrowth *in vitro*, positing that Loxl1 dysfunction and the ensuing impaired elastin synthesis during reactive astrocytosis in the ONH may contribute to impaired neuron-glia signaling in glaucoma. Our data support a role of dysregulated Loxl1 function in eliciting reactive astrocytosis in glaucoma subtypes associated with increased IOP, even in the absence of genetic polymorphisms in LOXL1 typically associated with exfoliation glaucoma. This suggests the need for a paradigm shift toward considering lysyl oxidase activity and elastin metabolism and signaling as contributors to an altered secretome of the ONH that may lead to the progression of glaucomatous changes. Future research is needed to investigate cargo of exosomes in the context of reactive astrocytosis and identify the pathways leading to the observed transcriptome changes during reactive astrocytosis.

1. Introduction

Glaucoma is a multifactorial progressive ocular pathology that manifests clinically with damage to the optic nerve (ON) and the retina, ultimately leading to blindness. Glaucoma develops with a characteristic three-step pathology that begins with remodeling of the optic nerve head (ONH), progresses to loss of ON axons, and ultimately results in degeneration of retinal ganglion cells (RGCs) (Calkins, 2012; Sharif,

* Corresponding author. Loyola University Chicago, 2160 South First Avenue, Center for Translational Research and Education, Visual Neurobiology and Signal Transduction Laboratory, Maywood, IL 60153, USA.
E-mail address: skaja@luc.edu (S. Kaja).

https://doi.org/10.1016/j.exer.2024.109813
Received 3 December 2023; Received in revised form 27 January 2024; Accepted 29 January 2024
Available online 6 February 2024
0014-4835/Published by Elsevier Ltd.

2018).

Primary open angle glaucoma (POAG) is the most common optic neuropathy in the United States and the leading cause of irreversible blindness worldwide (Kapetanakis et al., 2016). In POAG, elevated intraocular pressure (IOP) is widely considered the trigger for ONH remodeling and initiation of disease progression (Sharif, 2018; Weinreb et al., 2014, 2016).

The ONH shows the earliest signs of glaucoma pathology, and therefore, is an attractive target for drug discovery. In patients, ONH remodeling manifests as optic nerve cupping (Quigley et al., 1981; Quigley and Green, 1979), which precedes the loss of RGCs and associated vision loss (Harwerth and Quigley, 2006). However, the detailed molecular and biochemical changes associated with reactive astrocytosis in the ONH remain unknown.

Optic nerve head astrocytes (ONHA) are the primary cell type in the nonmyelinated ONH. Under physiological conditions, ONHA ensheath axons and provide homeostatic, trophic, metabolic and structural support. In response to pathological conditions, including biomechanical, bioenergetic and biochemical changes, ONHAs become activated and undergo a process referred to as reactive astrocytosis (Crawford Downs et al., 2011; Hernandez, 2000; Wang et al., 2017). While the exact role of reactive astrocytosis in central nervous system pathologies remains largely unknown, studies show that it can exert both beneficial and detrimental effects (Pekny and Pekna, 2014). In glaucoma patients, ONHA display a characteristic reactive phenotype (Wang et al., 2017), expression of glial fibrillary acid (GFAP; (Liu and Neufeld, 2000) and astrocyte remodeling has been shown to precede the ON axonopathy (Cooper et al., 2018). At the same time, inhibition of reactive astrocytosis by deletion of the transcription factor signal transducer and activator of transcription 3 (STAT3) from astrocytes exacerbated glaucomatous pathology (Sun et al., 2017). Collectively, these data suggest the presence of multiple pathways converging in molecular signatures attributed to reactive astrocytosis. Elucidation of the pathways underlying the molecular signatures of reactive astrocytosis and their contribution to optic neuropathy and axonopathy may result in the identification of novel molecular therapeutic targets for pharmacologic intervention in multiple subtypes of glaucoma.

The goal of this research was to elucidate the effects of reactive astrocytosis on the elastin metabolism pathway in primary rat ONHA. We identified a decrease in lysyl oxidase like 1 (*Loxl1*) expression in mechanical strain-induced reactive astrocytosis. We subsequently investigated the role of Loxl1 in reactive astrocytosis by generating primary rat ONHA cultures with decreased Loxl1 expression. Our results suggest that mechanical strain, similar to that experienced by patients with increased IOP, elicit molecular signatures of elastinopathy in ONHA through modulation of Loxl1. Interestingly, astrocyte derived exosomes (ADE) from Loxl1 deficient ONHA lost their trophic effects on neurite outgrowth *in vitro*. Further research in retinal ganglion cells, human cells, and *in vivo* systems is required, however, our data tentatively suggest the possibility that Loxl1 dysfunction and the ensuing impaired elastin synthesis during reactive astrocytosis in the ONH might contribute to impaired neuron-glia signaling in glaucoma.

2. Materials and methods

2.1. Cell culture

Primary rat ONHA were isolated and maintained as described by us previously (Ghosh et al., 2020; Kaja et al., 2015a, 2015b, 2017) in Dulbecco's modification of Eagle's medium supplemented with 4.5 g/L glucose, 4 mM L-glutamine, without sodium pyruvate (Corning, Thermo Fisher Scientific, Waltham, MA), 20% fetal bovine serum (FBS; Gemini Bio Products, West Sacramento, CA) and 1% penicillin/streptomycin (Gibco, Thermo Fisher Scientific, Waltham, MA) at 37 °C, 95% humidity and 5% CO_2. All cell culture plasticware was from TPP (Techno Plastic Products, Trasadingen, Switzerland). Cells from passages 5–26 were used for all experiments.

For exosome uptake assays, ONHA were seeded on 8-well chamber slides (Corning, Corning, NY) at a density of 3×10^4 cells/cm^2. Treatments were added after 48 h when cells had reached ~80% confluency and for up to 8 h.

Cultures with reduced Loxl1 expression were generated as described in Section 2.3. Below.

Primary E18 rat cortical neurons were purchased from Genlantis (Gene Therapy Systems Inc. San Diego, CA) and dissociated as described by us previously (Burroughs et al., 2012). Cells were maintained in Neurobasal A medium supplemented with B27 and GlutaMAX™ (all from Thermo Fisher Scientific, Waltham, MA) at 37 °C, 95% humidity and 5% CO_2. Cells were seeded on BioCoat® poly-D-lysine/laminin--coated 96-well plates or 8-well chamber slides (Corning, Corning, NY) at a density of 7.5×10^4 cells/cm^2. Exosome uptake assays were performed after 7 days in culture.

2.2. Exposure of ONHA cultures to equibiaxial mechanical strain

ONHA were seeded at a density of 2×10^4 cells/cm2 in 6-well Collagen I-coated BioFlex® Culture Plates (Flexcell International Corporation, Burlington, NC). Cells were grown to confluency (24–48 h), then the culture medium was replaced with serum-free medium and the plates were placed on the Flexcell FX-6000 Tension System (Flexcell International Corporation, Burlington, NC) and exposed to 10% static equibiaxial strain for 16 h, followed by a 2 h recovery period in a controlled atmosphere. Control cultures were placed in the same tissue culture incubator, without exposure to stretch.

2.3. Loxl1 knock-down (KD)

Transient Loxl1 KD was performed by transfection of Loxl1 small interference ribonucleic acid (siRNA) using Lipofectamine™ RNAiMAX Transfection Reagent (ThermoFisher Scientific, Waltham, MA), according to the manufacturer's instructions.

Chronic Loxl1 KD was achieved by lentiviral transduction of Loxl1 (SigmaAldrich, St Louis, MO; CSTVRS Mission shRNA Custom lentiviral particles). Non-targeting shRNA control (scramble) lentiviral particles were used as control. ONHA were plated in tissue culture coated 96 well plates at a density of 3×10^4 cell/cm^2. Cells were allowed to proliferate for 24 h and lentiviral particles were added to the cells at a multiplicity of infection (MOI) of 0.016. Media was changed after 48 h incubation with the viral particles. Transduction efficiency was determined by antibiotic selection by adding 7.5 μg/ml puromycin (Gemini Biosciences, West Sacramento, CA), as optimized by a puromycin cytotoxic curve.

2.4. Polymerase chain reaction (PCR)

Cell pellets were harvested from ONHA by scraping cells in ice-cold PBS. RNA isolation was performed using a Total RNA Purification Plus Kit (Norgen Biotek, Thorold, ON, Canada), according to the manufacturer's recommendations and as described previously (Ghosh et al., 2023). RNA concentration was measured by a nonospectrophotometer (ThermoFisher). cDNA was generated using the High Capacity cDNA Reverse Transcription Kit (Applied Biosciences, Thermo Fisher Scientific, Waltham, MA), as per the manufacturer's instructions. Quantitative PCR was performed using an AriaMx RT PCR System (Agilent Technologies, Santa Clara, CA) and Taqman® gene expression assays (ThermoFisher Scientific). Glyceraldehyde-3-phosphate dehydrogenase (GAPDH) was used as the housekeeping gene control in every reaction. Taqman® assays are listed in Suppl. Table 1. Data were analyzed by relative quantification using the $2^{-\Delta\Delta CT}$ method (Livak and Schmittgen, 2001).

2.5. Exosome isolation, characterization, and labeling

Astrocyte-derived extracellular vesicles (exosomes, ADE) were isolated by differential centrifugation of conditioned media (Luther et al., 2018; Thery et al., 2006). Conditioned media was centrifuged sequentially at 4 °C (2000×*g* for 20 min, 10,000×*g* for 30 min, 100,000×*g* for 2.5 h). The resultant exosome pellet was washed in 1 ml of Hank's Balanced Salt Solution (HBSS; Thermo Fisher Scientific), re-centrifuged at 100,000×*g* for 2.5 h, and then resuspended in 200 μl HBSS and stored at −80 °C.

Exosomal protein was quantified using the method of Lowry (Lowry et al., 1951) using bovine serum albumin as standard and converted to exosome number as described by us previously (Luther et al., 2018), where 1 μg total exosomal protein comprises 4.52×10^4 exosomes.

Exosomes were characterized by NanoSight NS300 (Malvern Instruments, Malvern, PA) using nanoparticle tracking analysis (NTA) by diluting ADE in HBSS and loading them into the instrument using a 1 ml tuberculin 31G syringe (Henke Sass Wolf, Tuttlingen, Germany) for size analysis.

Exosomes were labeled with SYTO™ RNASelect™ Green Fluorescent cell Stain (S32703; Thermo Fisher Scientific, Waltham, MA) fluorescent dye for ADE uptake assays. Fluorescent dye was added to ADE samples to a final concentration of 10 μM. Samples with dye were incubated at 37 °C for 20 min. Excess unincorporated dye was removed using Exosome Spin columns (Invitrogen, Thermo Fisher Scientific, Waltham, MA) following the manufacturer's instructions.

2.6. Immunocytochemistry and image acquisition

ONHA cultures were labeled for filamentous (F-) actin using AlexaFluor™ 488-conjugated phalloidin (Thermo Fisher Scientific, Waltham, MA) and actin fiber length was quantified using Matlab (Mathworks, Natick, MA, USA), as described by us in detail previously (Ghosh et al., 2020).

Immunocytochemistry was performed as described by us previously (Ghosh et al., 2020; Kaja et al., 2015b). Antibodies used for the presented studies are listed in Suppl. Table 2. Images were acquired using an SPE confocal microscope (Leica Microsystems, Buffalo Grove, IL).

For uptake experiments, cells were fixed in 4% paraformaldehyde (PFA) at room temperature for 20 min, washed and then permeabilized using 0.1% Triton X-100 (SigmaAldrich, St Louis, MO) at room temperature for 5 min. Cells were washed in PBS and mounted using Aqua-PolyMount (Polysciences Inc., Warrington, PA). Slides were imaged using a DeltaVision wide field fluorescent microscope (Applied Precision, GE) outfitted with a digital camera (CoolSNAP HQ2; Photometrics), equipped with an oil immersion Olympus Plan Apo 60× objective lens (1.42 numerical aperture) with Resolve™ immersion oil with a refraction index of 1.515 (Richard Allen Scientific, #M3004). Images were analyzed using ImageJ software (FiJi, National Institute of Health, Bethesda, MD).

Images from ADE uptake experiments and neuronal differentiation experiments were analyzed using the ImageJ software (Fiji) for mean fluorescence and the Neuron J plugin for mean neurite length (Meijering et al., 2004).

2.7. Immunoblotting

Exsomes isolated from primary optic nerve head astrocytes were lysed using a lysis buffer (0.5% w/v sodium dodecyl sulfate, 50 mM ammonium bicarbonate, 50 mM sodium chloride in dH_2O supplemented with HALT® protease inhibitor). ONHA were lysed in Cytobuster™ protein extraction reagent (Millipore Sigma, St. Louis, MO). Protein quantification was performed by Lowry assay using bovine serum albumin (BSA) (Bio-Rad Laboratories, Hercules, CA) as standard. Samples were diluted to the same concentration in lysis buffer. SDS-PAGE was performed in Laemmli buffer with and without 6% β-mercaptoethanol. Samples were denatured at 85 °C for 10 min. 6 μg of each protein sample was loaded on 15 well 4–12% NuPage Bis/Tris gels (Thermo Fisher Scientific, Waltham, MA) and electrophoresed at 150 V for 75 min. Samples were transferred from gels to nitrocellulose membrane (Amersham Protran, GE Healthcare, Chicago, IL) by wet transfer using methanol-free Western blot transfer buffer (Pierce®, Thermo Fisher Scientific, Waltham, MA) at 100 V for 80 min. Membranes were blocked in 5% milk in PBS with 0.2% Tween-20 (PBS-T) for 1 h 2.5% milk in PBS-T was used for primary antibody dilution and incubated overnight at 4 °C. The appropriate secondary antibodies were used in 2.5% milk at 1:20,000 dilution and incubated for 1 h at room temperature. Three washes of 5 min each were carried out with PBS-T after primary and secondary antibody incubations. Membranes were read using chemiluminescence with Luminata Forte reagent (Millipore Sigma, St. Louis, MO) and imaged using a ChemiDoc XRS + System (Bio- Rad Laboratories, Hercules, California). Data were analyzed in Image Lab software (Bio-Rad Laboratories, Hercules, California). Primary antibodies were rabbit anti-CD63 polyclonal antibody (PA5-92370, Thermo Fisher, Carlsbad, CA) and mouse anti-Alix monoclonal antibody (#2171, Cell Signaling Technology, Danvers, MA). Secondary antibodies were Amersham ECL horseradish peroxidase (HRP) conjugated anti-rabbit and anti-mouse antibodies (Cytiva, Marlborough, MA). Data were analyzed by densitometry with background correction and calculating the ratio of exosome to cell lysate expression.

2.8. Data analysis and statistics

All data were analyzed with the investigator blinded for treatment group. Data are presented as mean ± standard error of mean (SEM), geometric mean ± geometric standard deviation (SD) or as RQ ± R_{Qmin}/R_{Qmax}. Data were analyzed using one-tailed or two-tailed unpaired Student's t-test, One-Way ANOVA. Differences between groups on homoscedastic data sets were subsequently determined using Holm-Šidák's multiple comparisons test as appropriate. Differences were considered statistically significant at the $P < 0.05$ level. Statistical analysis was performed using GraphPad Prism 10.0.2 software (GraphPad Software, San Diego, CA, USA).

All experiments were performed using multiple technical and biological replicates. Only biological replicates, i.e. data from separate experiments, each using separate passages of cells and/or exosome preparations were used for statistical analysis and are indicated as n throughout the manuscript. Each n was derived from multiple technical replicates.

3. Results

3.1. Mechanical strain-induced reactive astrocytosis is associated with transcriptional changes in the elastin metabolism pathway

Exposure of ONHA to biomechanical forces that mimic increased IOP is a well-established insult that triggers reactive astrocytosis (Li et al., 2022; Lu et al., 2017). However, the effects of reactive astrocytosis on the elastin metabolism and signaling pathways remain largely unexplored. To address this knowledge gap, we exposed primary rat ONHA to 10% static equibiaxial mechanical strain for 16 h followed by a 2 h recovery period. Mechanical strain resulted in molecular and biochemical signatures characteristic of reactive astrocytosis, including a characteristic remodeling of the actin cytoskeleton that includes shortening of actin fibers and formation of crosslinked actin networks (Fig. 1A), and increase in GFAP expression (Fig. 1B), and an increase in cellular levels of Reactive Oxygen Species (ROS) (Fig. 1C).

Elastin synthesis involves two key extracellular matrix glycoproteins, fibrillin 1 (Fbn1), and fibulin 5 (Fbln5) and the deaminase activity of Loxl1, which activates tropoelastin thereby catalyzing its covalent crosslinking and formation of mature elastin fibers. Fibulin 2 (Fbln2) is associated with Fbn1, but has been shown to be dispensable for elastic

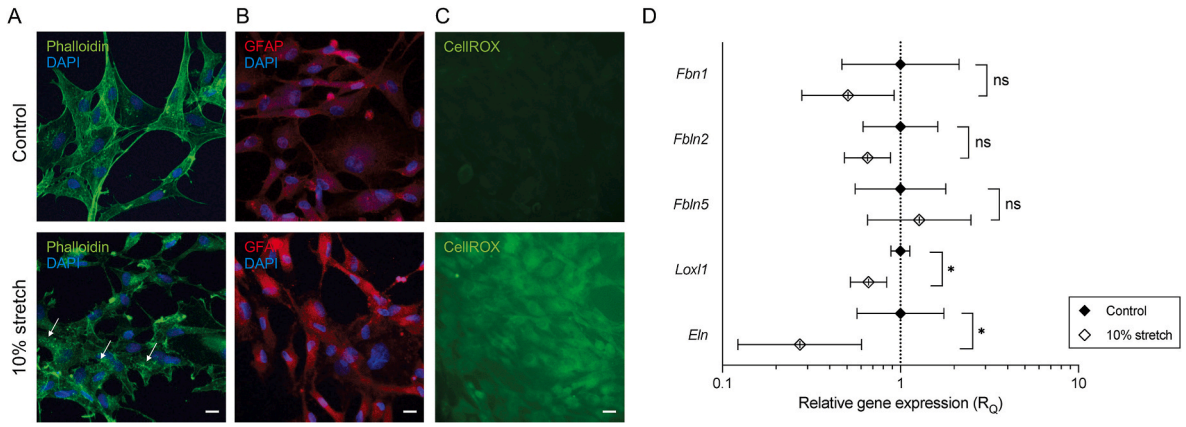

Fig. 1. Mechanical strain induced reactive astrocytosis is associated with gene expression changes in the Eln signaling pathway. A) Representative examples of phalloidin- and DAPI-labeled ONHA. Cytoskeletal remodeling is evident after exposure of ONHA to 10% static equibiaxial mechanical strain. Actin fibers are noticeably shortened, and cultures exhibited formation of crosslinked actin networks (arrows). Scale bar: 5 μm. **B)** Representative examples of GFAP immunoreactivity in ONHA exposed to mechanical strain. GFAP immunoreactivity was increased, confirming induction of reactive astrocytosis. Cells were co-labeled with DAPI. Scale bar: 5 μm. **C)** Reactive astrocytosis elicited by mechanical strain was associated with generation of oxidative stress. Representative images of ONHA labeled with CellROX™ are shown. Control ONHA showed only background fluorescence, while ONHA exposed to mechanical strain showed strong CellROX™ fluorescence indicative of ROS. Scale bar: 5 μm. **D)** Reactive astrocytosis was associated with statistically significant reductions in the gene expression of *Loxl1* and *Eln*, while expression of *Fbn1*, *Fbln2*, and *Fbln5* remained unaffected. Data are shown as relative gene expression (R_Q) ± R_{Qmin}/R_{Qmax}. *$P < 0.05$.

fiber formation (Sicot et al., 2008). Mechanical strain-induced reactive astrocytosis resulted in statistically significant reductions in the expression *Loxl1* (44% decrease, n = 3, $P < 0.05$) and *Eln* (73% decrease, n = 3, $P < 0.05$) gene expression (Fig. 1D). In contrast, expression of *Fbn1* ($P = 0.15$), *Fbln2* ($P = 0.13$), and *Fbln5* ($P = 0.33$) remained unaffected (Fig. 1D).

This novel finding of reduced elastin expression in ONHA response to biomechanical insult is consistent with our findings in glaucomatous DBA/2 J mice, which exhibit significantly reduced elastin expression in the ONH, but not the mylelinated ON region (Suppl. Fig. 1).

3.2. *Loxl1 KD is sufficient to induce reactive astrocytosis in ONHA*

Our novel finding of decreased *Loxl1* expression in ONHA following mechanical strain insult prompted us to investigate whether reduced cellular Loxl1 levels are sufficient to elicit phenotypes of reactive astrocytosis. To this end, we used *Loxl1* targeted siRNA to transiently reduce Loxl1 levels. *Loxl1* gene expression was reduced by 58% (n = 3, $P < 0.01$; Fig. 2A) and accompanied by a marked reduction in Loxl1 immunoreactivity in ONHA (Fig. 2B). Concomitantly, GFAP expression increased 2.2-fold (n = 14, $P < 0.01$; Fig. 2C–D). We further observed changes in the actin cytoskeleton consistent with reactive astrocytosis (Ghosh et al., 2020). Specifically, F-actin fiber length was significantly decreased in *Loxl1* KD vs. scramble ONHA (n = 4, $P < 0.01$; Fig. 2E–F). Taken together, these data suggest that reduced Loxl1 levels are sufficient to elicit reactive astrocytosis in ONHA.

We next investigated whether *Loxl1* KD resulted in changes to the elastin metabolism pathway. Notably, *Eln* gene expression was reduced by 29% (n = 3, $P < 0.01$; Fig. 3A), which was accompanied by a marked reduction in Eln immunoreactivity as assessed by immunocytochemistry (Fig. 3B). Expression of *Fbln5* (Fig. 3C) and *Fbn1* (Fig. 3D) were not changed in Loxl1 KD ONHA; mRNA levels of *Fbln2* showed a small (21%), yet significant reduction compared to scramble control ONHA (n = 3, $P < 0.05$; Fig. 3E).

Our data suggest a putative role for Loxl1 in reactive astrocytosis, and partial loss of Loxl1 appears sufficient to trigger reactive astrocytosis in cultured ONHA. Notably, the observed reduction in Eln expression was similar to that observed in response to mechanical strain.

3.3. *Astrocyte-derived exosomes are readily taken up by both ONHA and neurons*

Recently, the role of exosomes, a subtype of extracellular vesicles, in intercellular communication has gained significant attention. However, there is limited knowledge to what extent ONHA secrete exosomes and what cell types can take up exosomes. Furthermore, data support a role for the extracellular matrix to regulate the secretion and uptake of exosomes, while at the same time, cargo of exosomes has been shown to remodel the extracellular matrix in cancer (for review, see Karampoga et al., 2022). We hypothesized that ONHA produce exosomes, which may be taken up by both astrocytes and neurons, and further, that reduced Loxl1 levels in ONHA may alter the functional properties of these ADE.

To test our hypothesis, we isolated exosomes from ONHA cultures using established and validated ultracentrifugation protocols (Luther et al., 2018; Thery et al., 2006).

We labeled exosomes using an RNA-specific nucleic acid stain (SYTO™ RNASelect™) that is readily taken up into exosomes and exhibits bright fluorescence (absorption/emission maxima ~490 nm/530 nm) when bound to RNA. We subsequently quantified fluorescence intensity as a surrogate of exosome uptake. In a first experiment, we determined ADE uptake at 8 h following exposure of ONHA to 1×10^6 ADE. We used rigorous experimental controls, including a negative control (dye processed in an identical way to exosomes, including column purification; "Dye Control") and a positive control (dye dissolved in saline; "Dye Only") to determine the dynamic range of the assay. Fluorescence data were normalized to the Dye Control condition. ADE added to ONHA resulted in an ~2-fold increase of cellular fluorescence compared with unlabeled exosomes (n = 3; $P < 0.05$; Fig. 4A). The positive control resulted in an ~3.6-fold increase of fluorescence (n = 3; $P < 0.001$; Fig. 4A).

We next determined the time-course of ADE uptake into ONHA for up to 8 h. Exposure of ONHA to ADE resulted in a time-dependent uptake of ADE into ONHA that continued to increase over an 8 h period (Fig. 4B–C).

To evaluate the ability of neurons to take up ADE, we exposed cultures of rat primary cortical neurons to ADE (1×10^6 ADE per well). We performed our initial control experiments at 8 h, which resulted in ~1.6-fold increase in fluorescence in neurons treated with labeled ADE (n = 3, $P < 0.01$; Fig. 5A). We further evaluated the time course of ADE uptake

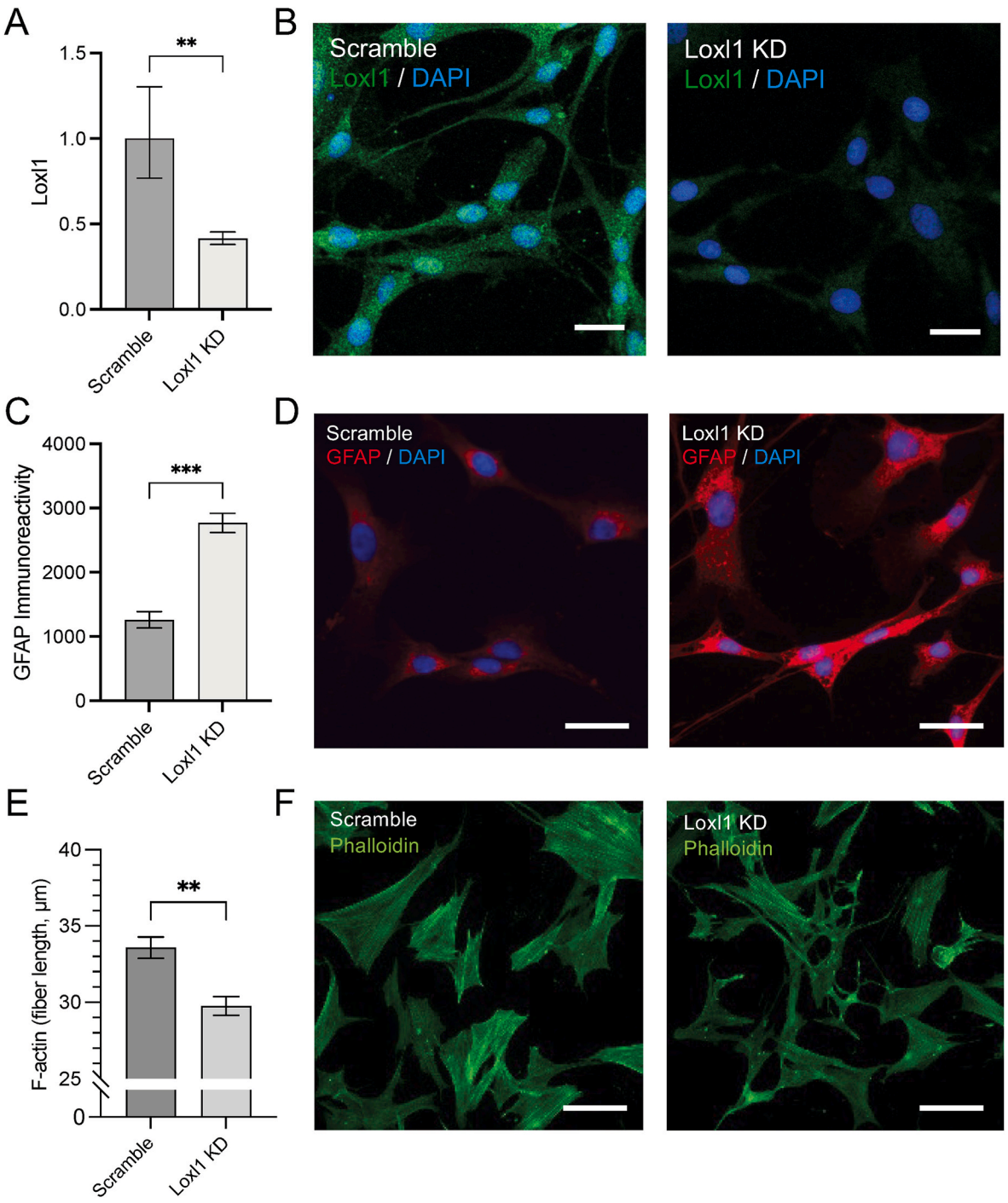

Fig. 2. Loxl1 KD results is sufficient to increase GFAP immunoreactivity, suggestive of reactive astrocytosis. **A)** *Loxl1* expression was decreased by 58% following transfection with *Loxl1* targeted siRNA. **B)** Representative images of Loxl1 immunoreactivity confirmed successful Loxl1 KD in ONHA. Cells were co-labeled with DAPI. **C)** Concomitantly, GFAP immunoreactivity increased 2.2-fold, suggestive of activation of ONHA. **D)** Representative images of GFAP immunoreactivity are shown. **E)** Actin fiber length was significantly reduced in *Loxl1* KD ONHA compared with scramble-transfected ONHA. **F)** Representative examples of phalloidin-labeled ONHA. Cytoskeletal remodeling is evident and actin fibers are noticeably shortened. Scale bar: 10 µm $^{**}P < 0.01$, $^{***}P < 0.001$.

into neurons for up to 8 h. ADE uptake peaked at 4 h (n = 3, $P < 0.05$; Fig. 5B–C) and the fluorescent signal returned to baseline after 8 h.

3.4. *Loxl1 deficiency does not alter physiochemical properties of ADE*

Based on these findings, we set out to test the hypothesis that Loxl1 deficiency in ONHA may alter either or both the physiochemical and functional effects of ADE. To test this hypothesis, we generated ONHA cultures with reduced Loxl1 expression using lentivirus delivery of Loxl1-targeting shRNA. We targeted a Loxl1 expression level of 50% of naïve ONHA, as previously described for ON tissue from exfoliation glaucoma patients (Schlotzer-Schrehardt et al., 2012), which was accomplished by transduction using an MOI of 0.016 (Suppl. Fig. 2).

We performed NTA to characterize of ADE using the Nanosight instrument. There was no difference in the size distribution between ADE from naïve ONHA ($ADE^{Naïve}$), ONHA transduced with a lentivirus expressing a non-targeting shRNA ($ADE^{Scramble}$), and ONHA with transduced with a lentivirus expressing *Loxl1*-targeting shRNA resulting

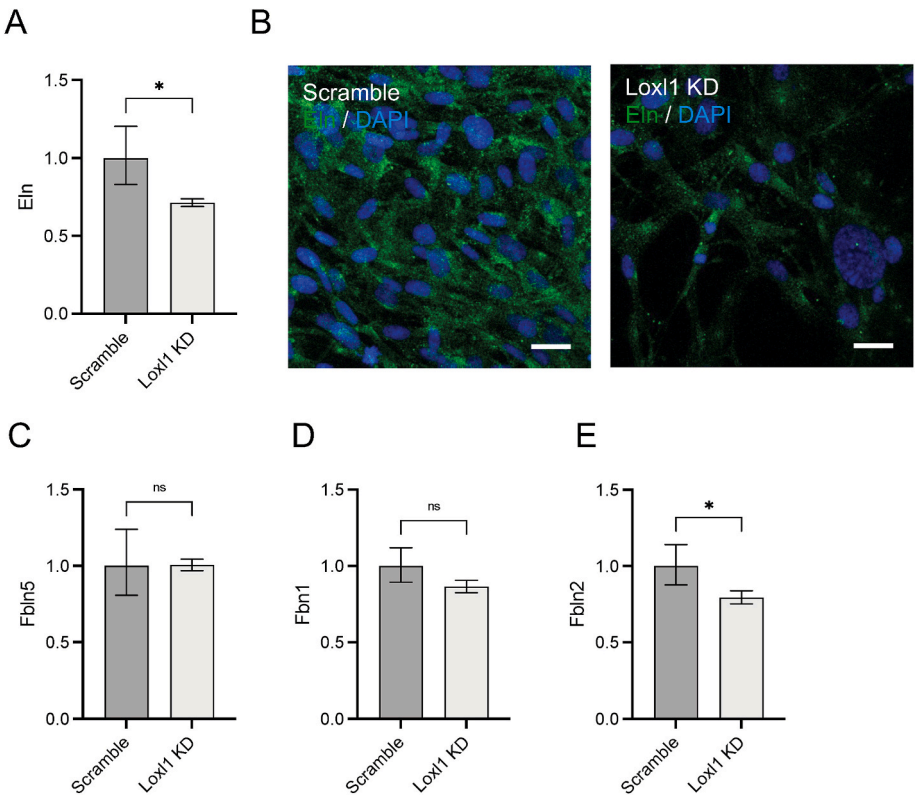

Fig. 3. Loxl1 deficiency results in decreased Eln expression. A) Loxl1 KD resulted in a 29% decrease of *Eln* gene expression. **B)** This was accompanied by a marked reduction in Eln immunoreactivity in ONHA. Cells were co-labeled with DAPI. Representative images are shown. Scale bar: 10 μm. **C)** *Fbln5* expression was unaffected by Loxl1 KD. **D)** Similarly, Loxl1 KD had no effect on *Fbn1* expression. **E)** Expression of *Fbln2* was decreased by 21% following Loxl1 KD. *$P < 0.05$; ns, not significant.

in ~50% reduced Loxl1 expression ($ADE^{Loxl1\ KD}$) (Fig. 6A). Specifically, we fitted a Gaussian distribution for each sample and compared the amplitude (n = 3, $P = 0.99$), the mean (n = 3, $P = 0.95$) and standard deviation (n = 9, $P = 0.59$) of the Gaussian fit. Mean exosome size was ~120 nm and not statistically significant different between the three experimental groups as determined by NTA (n = 3, $P = 0.90$; Fig. 6B).

Expression of exosome markers was assessed by immunoblotting of ADE lysates. All three ADE expressed the prototypic exosome markers, Alix and CD63, which were detectable in cell and exosome lysates (Fig. 6C). The tetraspanin, CD81, was not identified in any of the three ADE lysates (data not shown). There was no significant difference in normalized Alix expression (n = 3; ANOVA, $P = 0.99$, Fig. 6D).In contrast, normalized CD63 expression was lower in both $ADE^{Scramble}$ and $ADE^{Loxl1\ KD}$, compared with $ADE^{Naïve}$ (n = 3; ANOVA, $P < 0.001$, Fig. 6E).

3.5. *Loxl1-deficient ADE exerted diminished functional effects on neurite outgrowth in vitro*

We continued to investigate the functional effects of ADE by quantifying neurite outgrowth of primary rat cortical neurons following exposure to ADE during neuronal development *in vitro*. ADE were added to neuronal culture on days 3 (D3) and 5 (D5) in culture at a concentration of 100 μg/ml in 100 μl total volume, equivalent to 0.45×10^6 ADE per well. Neurite outgrowth was quantified on day 7 (D7) in culture (Fig. 7A).

Addition of $ADE^{Naïve}$ to neuronal cultures resulted in a significant increase in neurite outgrowth by 20.1 ± 3.3 μm compared to neuronal cultures without ADE addition (n = 5, $P < 0.05$, Fig. 7B–C). $ADE^{Scramble}$ elicited a similar increase in neurite growth (18.7 ± 2.0 μm; n = 5, $P = 0.85$; Fig. 7B–C) compared to the $ADE^{Naïve}$ condition. In contrast, $ADE^{Loxl1\ KD}$ did not lead to an increase in neurite outgrowth (2.23 ± 4.0 μm), and neurite outgrowth was significantly less compared to the $ADE^{Scramble}$ group (n = 5, $P < 0.05$; Fig. 7B–C).

4. Discussion

In this study, we investigated the effect of mechanical strain-induced reactive astrocytosis on elastin expression in primary rat ONHA. We discovered dysregulated gene expression of components of the elastin metabolism pathway, most notably a reduction in *Loxl1* expression. Decreased *Loxl1* expression was sufficient to induce reactive astrocytosis in ONHA, resulting in decreased *Eln* expression and Eln immunoreactivity. ADE were readily taken up by both ONHA and primary cortical neurons. $ADE^{Loxl1\ KD}$, derived from Loxl1-deficient ONHA, exhibited diminished functional effects on neuronal differentiation, specifically neurite outgrowth, compared with $ADE^{Scramble}$ and $ADE^{Naïve}$.

Reactive astrocytosis was induced by exposure to ONHA to equibiaxial mechanical strain, which is a well-established method to elicit reactive phenotypes in astrocytes. We selected the experimental conditions used for the experiments presented herein based on our own preliminary studies (Kaja et al., 2020) and work by others that have reported phenotypes of reactive astrocytosis following 10% static mechanical strain. For example, a similar rearrangement of the actin cytoskeleton in response to stimulation by 10% mechanical strain was previously reported (Li et al., 2022). Notably, the observed phenotypes of reactive astrocytosis are consistent with previous work by us and others (Ghosh et al., 2020; Liu et al., 2022). We have previously demonstrated that short exposure to mechanical strain (4 h), an experimental paradigm uniquely suited to quantify the effect of biomechanical strain on second messengers and cytokines, leads to pannexin-mediated increases in adenosine triphosphate (ATP), which elicits P2X7 receptor activation and consequent increases in interleukin-6 (IL-6) expression and secretion (Lu et al., 2017). Exposure

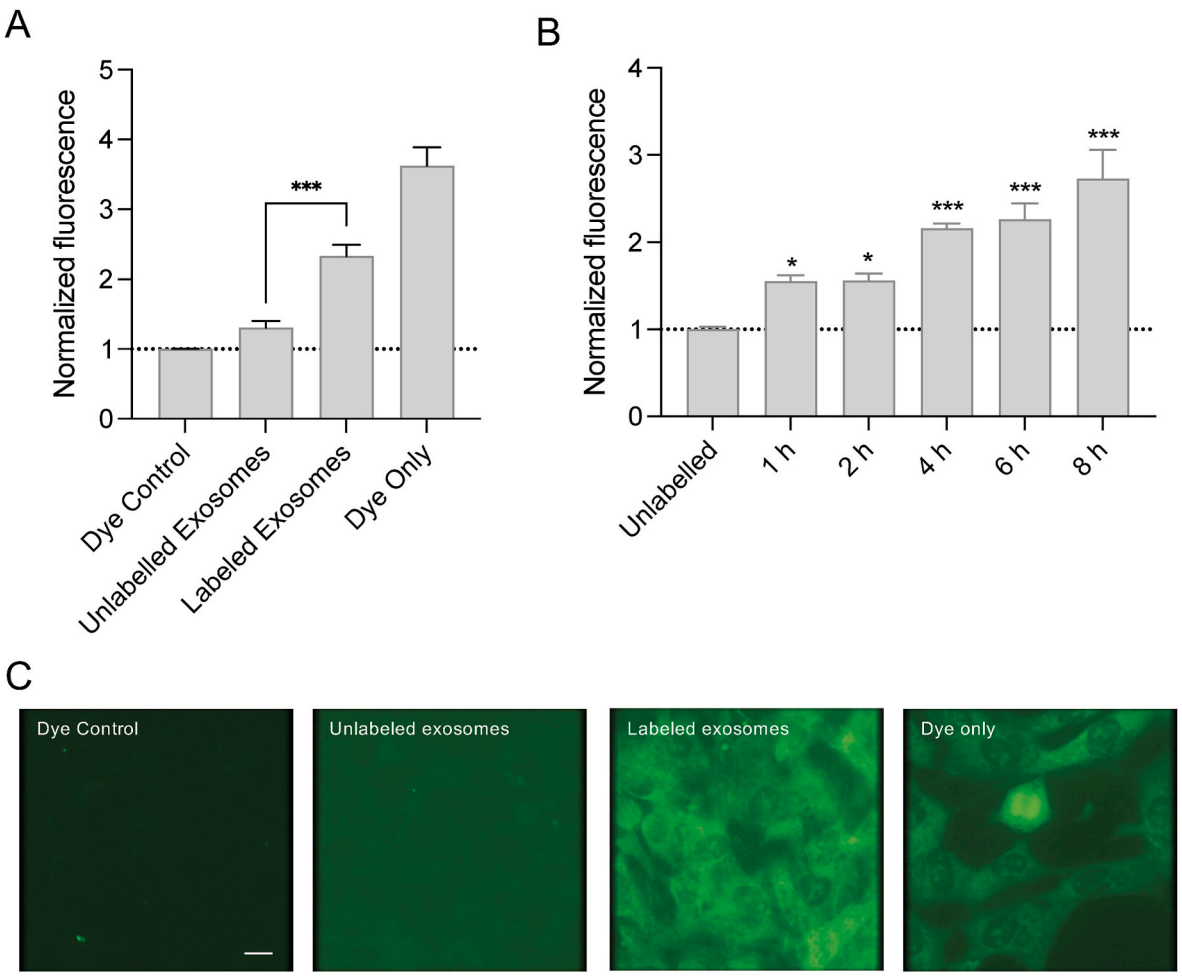

Fig. 4. Exosome uptake by ONHA. A) Exosomes were labeled with an RNA-specific nucleic acid stain (SYTO™ RNASelect™). ADE uptake was quantified after 8 h, which resulted in a significant increase in fluorescence. Dye Control and Dye Only conditions were used as negative and positive controls, respectively. **B)** To determine the time course of ADE uptake, ONHA were exposed to ADE over an 8 h period during which fluorescence steadily increased. **C)** Representative examples of ONHA at 8 h are shown. Scale bar: 5 μm $^{*}P < 0.05$, $^{***}P < 0.001$.

to cyclic mechanical strain (24 h, 12%, 1 Hz) has revealed changes to ONHA bioenergetics, including greater extracellular acidification and lower ATP-linked respiration, yet higher maximal respiration and spare capacity in stretched optic nerve head astrocytes (Pappenhagen et al., 2022).

While equibiaxial strain models the biomechanical forces upon the optic nerve head associated with elevated intraocular pressure in glaucoma, the model also has significant limitations. These include applying strain to a monoculture of ONHA, single-substrate growth surfaces, and selection of a single time-amplitude combination of mechanical strain. Future multiparametric studies are needed to further investigate the effects of mechanical strain on ONHA and elastin metabolism.

In vivo research has reported numerous phenotypes associated with reactive astrocytosis. In the mouse microbead model, astrocytes close to the myelination transition zone were found to extend new processes that follow the longitudinal axis of the ON and invade axon bundles (Wang et al., 2017). Recent RNA-sequencing and single-cell PCR experiments indicate that increased astrocytic phagocytosis is an early event following ocular hypertension (Zhu et al., 2023). Interestingly, a significant amount of functional heterogeneity was identified in the astrocytes of the glial lamina, and notably, signs of reactivity were identified in naïve nerves (Zhu et al., 2023), providing a scientific basis for the experimental variability typically observed when studying reactive astrocytes. The role of biomechanical forces in triggering reactive astrocytosis was elegantly demonstrated in a rat model that combined controlled elevation of intraocular pressure with retrobulbar optic nerve transection, where ocular hypertension was required to trigger ONH astrocyte changes in structural orientation (Tehrani et al., 2019). These experimental findings are representative of changes observed in astrocytes from glaucomatous donors (Hernandez, 2000; Hernandez et al., 2002; Varela and Hernandez, 1997), and support the generally accepted notion that reactive astrocytosis is an early process in the pathophysiology of primary open angle glaucoma.

Yet, which features of reactive astrocytosis are beneficial *vs*. detrimental to glaucoma progression remains unknown. While oxidative stress is generally be considered a detrimental component of reactive astrocytosis (Fan Gaskin et al., 2021; Shim et al., 2018), knockout of signal transducer and activator of transcription 3 (STAT3) from astrocytes resulted in attenuated astrocyte hypertrophy and reactive remodeling (Sun et al., 2017).

Our data are based on the novel finding that reactive astrocytosis in ONHA is associated with a decrease in *Loxl1* and *Eln* expression. LOXL1 is a copper-dependent monoamine oxidase required for cross-linking collagen and elastin fibers in the extracellular matrix and multiple single nucleotide polymorphisms in the *LOXL1* gene are associated with exfoliation glaucoma (for review, see (Li et al., 2021; Schlotzer-Schrehardt and Zenkel, 2019). Exfoliation glaucoma is generally considered to be the result of accumulating pseudoexfoliative material, visible at pupillary margin and anterior lens capsule, which obstructs the trabecular meshwork leading to increased IOP (Naumann et al., 1998;

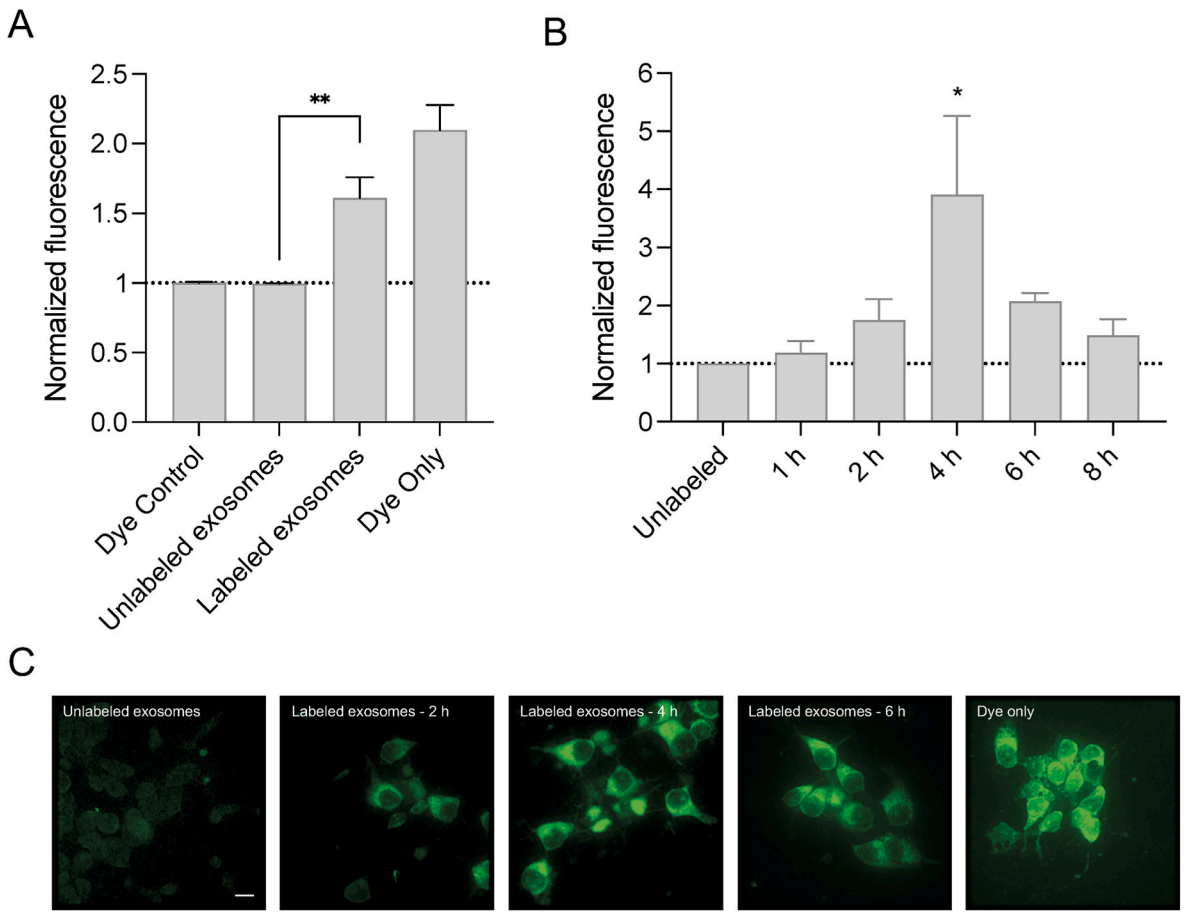

Fig. 5. Exosome uptake by primary cortical neurons. A) Primary E18 rat cortical neurons were exposed to ADE for 8 h, which resulted in ~1.6-fold increase in fluorescence in neurons treated with labeled ADE. **B)** When investigating the time course of ADE uptake into neurons, fluorescence peaked at 4 h and had returned to baseline after 8 h. **C)** Representative examples of ADE uptake into neurons are shown. Scale bar: 5 μm $^{*}P < 0.05$, $^{**}P < 0.01$.

Yuksel and Yilmaz Tugan, 2023). It has been proposed that pseudoexfoliation syndrome, and exfoliation glaucoma, are a form of elastinopathy (Plateroti et al., 2015; Schlotzer-Schrehardt et al., 2012; Schlotzer-Schrehardt and Zenkel, 2019).

Elastin is a critical component of the extracellular matrix and confers biomechanical compliance to the ONH and is a mediator of several important intracellular and extracellular signaling pathways (Navneet and Rohrer, 2022). We here found a reduction in *Eln* gene expression in cultured ONHA exposed to mechanical strain and in the presence of reduced Loxl1 levels. Furthermore, Eln immunoreactivity was significantly reduced in the glaucomatous ONH of DBA/2 J mice.

Interestingly, both *LOXL1* and *ELN* expression were significantly reduced in the lamina of exfoliation glaucoma patients (Schlotzer-Schrehardt et al., 2012). Although *LOXL1* expression was reduced in the lamina of POAG patients, this difference did not reach statistical significance in this study (Schlotzer-Schrehardt et al., 2012), likely attributable to the small number of POAG samples investigated. Nonetheless, these data offer clinical support for our novel finding of reduced *Loxl1* expression in reactive ONHA. In contrast, there are numerous conflicting reports pertaining to the presence of abnormal elastin fibers and the presence of elastosis in POAG (Pena et al., 1998; Quigley et al., 1991, 1996; Varela and Hernandez, 1997).

The signaling pathways that regulate *Eln* and *Loxl1* expression remain unknown. While reduced Loxl1 activity can readily be linked to impaired assembly of mature elastin fibers, one can only speculate how reduced Loxl1 levels elicit reduced *Eln* gene expression. Elevated levels of transforming growth factor beta (TGFβ) result in enhanced extracellular matrix synthesis. The ensuing fibrosis in ocular tissues, including the ONH, has been proposed as contributing factor to glaucoma pathogenesis (Fuchshofer, 2011; Fuchshofer and Tamm, 2012; Wallace and O'Brien, 2016). TGFβ signaling is known to increase LOXL1 via Smad2/3-mediated signaling (Fuchshofer and Tamm, 2012; Kim et al., 2018; Sethi et al., 2011). Intriguingly, LOX, an isoform of LOXL1, has been proposed to be a negative regulator of TGFβ (Atsawasuwan et al., 2008; Kutchuk et al., 2015). It is thus possible that reduction of LOXL1 expression is a cellular anti-fibrotic response early during reactive astrocytosis. Furthermore, the presence of pro-inflammatory cytokines and modulators, such as prostaglandin E2, has been shown to decrease LOX1 levels in fibroblasts, however, it is not known if a similar mechanism exists in ONHA (Liu et al., 2016; Roy et al., 1996; Yokoyama et al., 2014).

To our knowledge, this report is the first investigating the properties of ADE from the ONH. Extracellular vesicles express a number of proteins, including members of the tetraspanin family (CD9, CD63 and CD81), the endosomal sorting complex required for transport (ESCRT) proteins Alix and TSG101, in addition to members of the integrin, heat shock protein, flotillin, and cytoskeletal families of proteins (Gurung et al., 2021; Zhang et al., 2019). CD63, ESCRT and cytoskeletal components are generally considered common among all exosomes (Mashouri et al., 2019) and Alix and tetraspanins are the best-established markers of exosomes (Kalra et al., 2012; Thery et al., 2009; van Niel et al., 2018). Therefore, we herein probed for Alix, CD63, and CD81 in ADE.

Alix expression was similar between $ADE^{Naïve}$, $ADE^{Scramble}$ and $ADE^{Loxl1\ KD}$, however, we did identify a significant decreased in CD63 expression in lentivirus-transduced ONHA. However, no difference in

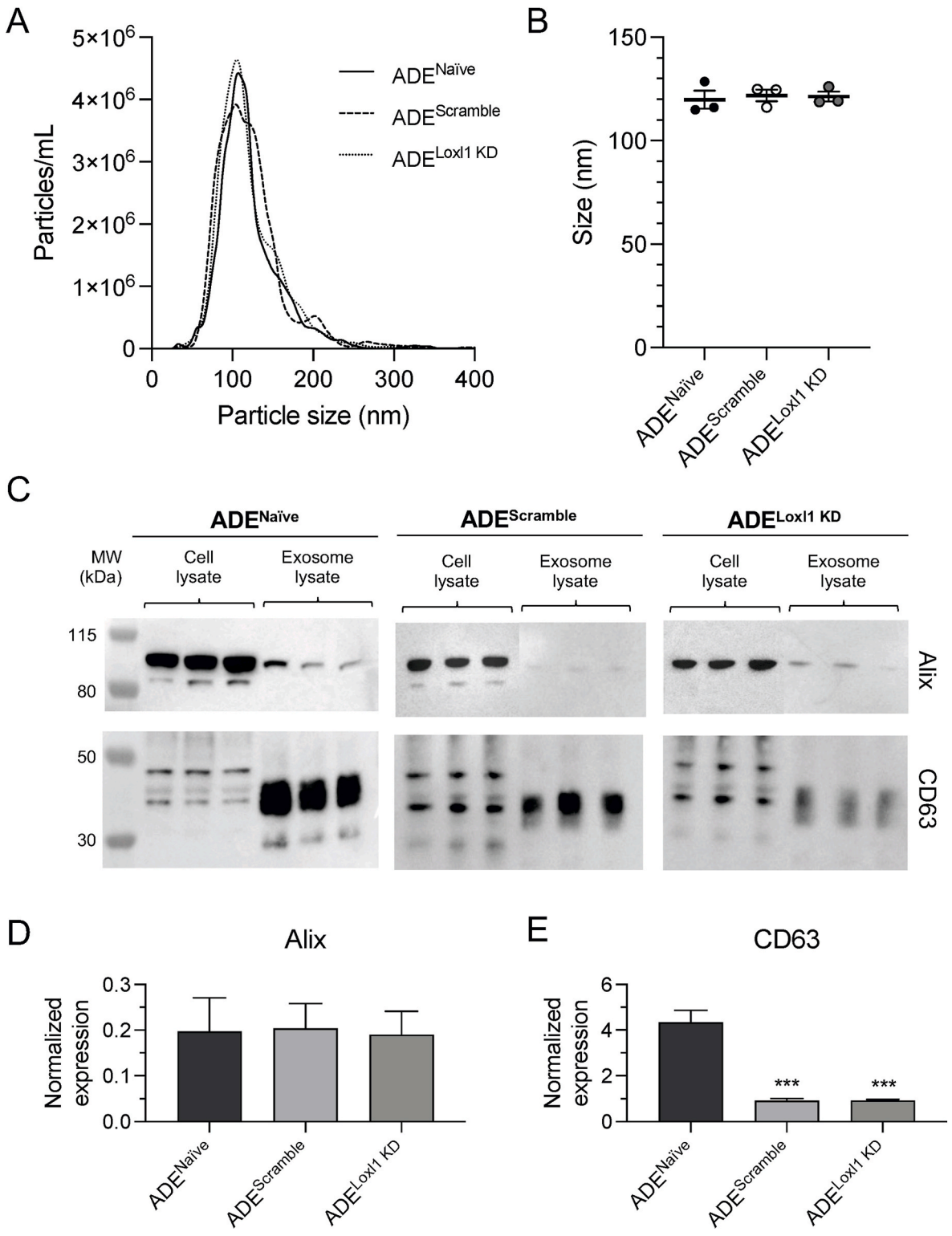

Fig. 6. Characterization of exosomes. A) ADE were characterized by NTA to determine possible differences in size distribution between $ADE^{Naïve}$, $ADE^{Scramble}$, $ADE^{Loxl1\ KD}$. No statistically significant differences in amplitude, mean, and standard deviation were identified. **B)** Mean exosome size was ~120 nm and did not differ between ADE populations. **C)** Expression of exosome markers was assessed by immunoblotting of cell and ADE lysates. Representative immunoblots of Alix and CD63 are shown. **D)** Expression of Alix did not differ between ADE populations as assessed by the ratio of background-corrected exosome to cellular lysate levels. **E)** CD63 expression was significantly reduced in $ADE^{Scramble}$ and $ADE^{Loxl1\ KD}$, compared with $ADE^{Naïve}$. $^{***}P < 0.001$.

expression between $ADE^{Scramble}$ and $ADE^{Loxl1\ KD}$ was found, making it unlikely that a change in CD63 is responsible for the differential functional effects of these ADE populations. Rather, it is likely that changes in CD63 are associated with lentiviral transduction.

ADE were taken up readily by ONHA and primary neurons *in vitro*, enabling a role of ADE in neuron-glia signaling in the ONH. Various different types of exosomes have been used as therapeutic modalities in preclinical ocular disease models, however, the focus has been on the

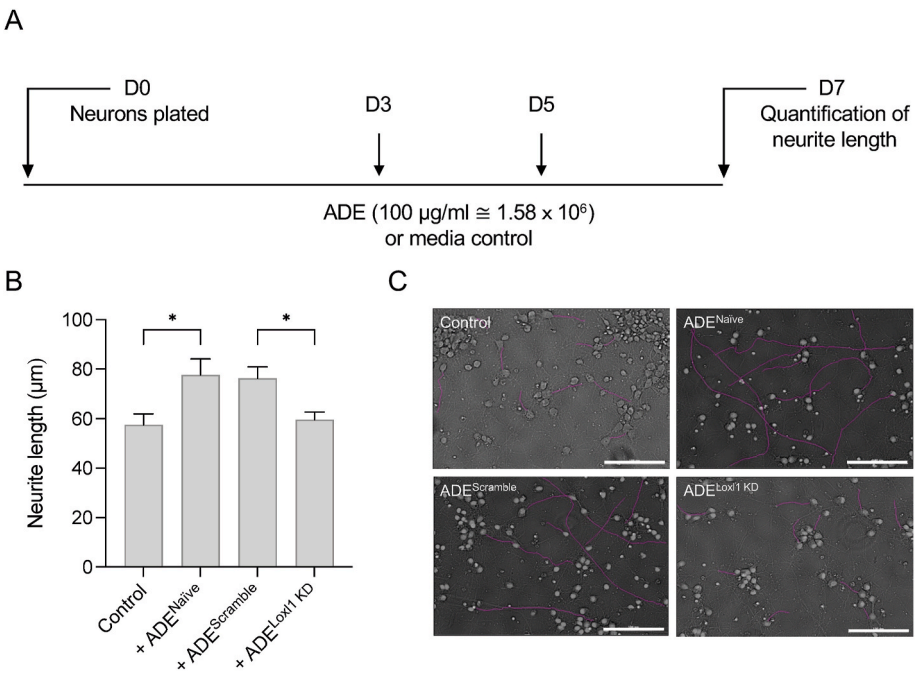

Fig. 7. ADE^{Naïve} enhance primary neurite length *in vitro*, while ADE$^{Loxl1\ KD}$ are devoid of functional effects on neurite outgrowth. **A)** ADE were added to neuronal cultures on days 3 (D3) and 5 (D5) in culture at a concentration of 100 µg/ml (equivalent to 1.58 × 10^6 ADE per well). Neurite outgrowth was quantified on day 7 (D7) in culture. A graphical depiction of the experimental design is shown. **B)** Addition of ADE^{Naïve} to neuronal cultures resulted in a significant increase in neurite outgrowth. ADE^{Scramble} elicited similar functional effects as ADE^{Naïve}. In contrast, ADE$^{Loxl1\ KD}$ did not elicit increased neurite outgrowth and neurite length was similar to the Control condition. **C)** Representative examples of neurite outgrowth quantification are shown. Primary dendrites are traced in magenta. Scale bar: 100 µm $^*P < 0.05$.

therapeutic properties of mesenchymal stem cell derived exosomes (for review, see (Liu et al., 2020; Wu et al., 2023). Pioneering work has shown that bone marrow-derived mesenchymal stem cell-derived exosomes can promote RGC survival in the optic nerve crush model (Mead and Tomarev, 2017) and the DBA/2 J strain with pigmentary glaucoma (Mead et al., 2018). Interestingly, fibroblast-derived exosomes did not protect against RGC loss (Mead and Tomarev, 2017).

ADE have received more attention in brain disorders and numerous studies have revealed neurotoxic and neuroprotective effects, as recently reviewed in detail (Zhao et al., 2021). ADE delivered systemically by intravenous injections were protective in a rat model for traumatic brain injury through modulation of the endogenous antioxidant pathway (Zhang et al., 2021), supporting functional roles of ADE in neuron-glia signaling. As such, these data offer precedent for the functional effects of ONHA-derived ADE reported in the present study. Specifically, our data on the functional effects of ADE on neuronal outgrowth suggest a role for ADE on the extracellular matrix thereby enhancing neurite formation.

One limitation of our study is the use of rat primary cortical neurons rather than RGC to evaluate the functional effects of ADE. For this initial study, we selected cortical neurons due to their faster *in vitro* differentiation and lesser biological variability. Current ongoing research is investigating the functional effects on RGC. In this study, we only evaluated the effects of ADE from ONHA with reduced Loxl1 expression. Future studies are needed to characterize ADE from ONHA exposed to mechanical strain.

Elastin degradation has been proposed to play an important role in initiating neurodegenerative deficits in neurodegenerative disease, including Alzheimer's disease (for review, see (Soles et al., 2023). However, studies investigating the specific contributions of elastin to the extracellular matrix and their effect on neurite outgrowth remain elusive. Exosomes can stimulate elastin synthesis, which has led to their proposed use as therapeutics for among other dermatologic disease (Shi et al., 2021; Thakur et al., 2023), and served as rationale for studying the effects of ADE on neurite outgrowth.

Our data suggest a role of dysregulated LOXL1 function in reactive astrocytosis and subtypes of glaucoma associated with increased IOP, including POAG, even in the absence of genetic polymorphisms in LOXL1 typically associated with exfoliation glaucoma. This suggests a need for a paradigm shift toward considering LOXL1 activity and ELN metabolism as contributors to an altered secretome of the ONH that may lead to the progression of glaucomatous changes. Future research is needed to investigate astrocyte-derived exosomal cargo in the context of reactive astrocytosis and identify the molecular alterations in ADE$^{Loxl1\ KD}$ responsible for the loss of functional effects.

Funding

This research was funded in part by The Glaucoma Foundation (S.K.), the Illinois Society for the Prevention of Blindness (A.K.G., H.N.H., S.M.R.), NIH (grants EY013434, EY015537, EY001583; C.H.M. and EY020496; R.M.S), the Wake Forest Translational Eye and Vision Research Center (R.M.S.), Eversight (S.K.), the Dr. John P. and Therese E. Mulcahy Endowed Professorship in Ophthalmology (S.K.), the Richard A. Perritt M.D. Charitable Foundation (S.K.), K&P Scientific LLC (A.K.G., S.K.) and the Department of Veterans Affairs (grant I21RX001593; E.B.S.). This material is the result of work supported with resources and the use of facilities at the Edward Hines Jr. VA Hospital, Hines, IL. The contents do not represent the views of the U.S. Department of Veterans Affairs or the United States Government.

Disclosures

The authors disclose no financial conflicts of interest.

CRediT authorship contribution statement

Harsh N. Hariani: Writing – review & editing, Writing – original

draft, Methodology, Investigation, Funding acquisition, Formal analysis, Data curation, Conceptualization. **Anita K. Ghosh:** Writing – review & editing, Validation, Supervision, Project administration, Methodology, Investigation, Funding acquisition, Formal analysis, Conceptualization. **Sasha M. Rosen:** Writing – review & editing, Methodology, Investigation. **Huen-Yee Tso:** Writing – review & editing, Investigation. **Cassidy Kessinger:** Writing – review & editing, Writing – original draft, Visualization, Methodology, Investigation. **Chongyu Zhang:** Writing – review & editing, Validation, Supervision, Formal analysis. **W. Keith Jones:** Writing – review & editing, Writing – original draft, Validation, Supervision, Resources, Project administration, Methodology, Investigation, Funding acquisition, Formal analysis, Conceptualization. **Rebecca M. Sappington:** Conceptualization, Formal analysis, Funding acquisition, Investigation, Writing – review & editing. **Claire H. Mitchell:** Writing – review & editing, Supervision, Software, Methodology, Investigation. **Evan B. Stubbs:** Writing – review & editing, Validation, Supervision, Resources, Project administration, Funding acquisition, Data curation. **Vidhya R. Rao:** Writing – review & editing, Writing – original draft, Validation, Supervision, Methodology, Investigation, Funding acquisition, Formal analysis, Data curation. **Simon Kaja:** Writing – review & editing, Writing – original draft, Visualization, Validation, Supervision, Software, Resources, Project administration, Methodology, Investigation, Funding acquisition, Formal analysis, Data curation, Conceptualization.

Data availability

Data will be made available on request.

Acknowledgements

The authors would like to thank Dr. Ed Campbell for making his DeltaVision microscope available for these studies. The numerous volunteers in the Visual Neurobiology and Signal Transduction Laboratory are acknowledged for their contributions to our ongoing research program.

Appendix A. Supplementary data

Supplementary data to this article can be found online at https://doi.org/10.1016/j.exer.2024.109813.

References

Atsawasuwan, P., Mochida, Y., Katafuchi, M., Kaku, M., Fong, K.S., Csiszar, K., Yamauchi, M., 2008. Lysyl oxidase binds transforming growth factor-beta and regulates its signaling via amine oxidase activity. J. Biol. Chem. 283, 34229–34240.
Burroughs, S.L., Duncan, R.S., Rayudu, P., Kandula, P., Payne, A.J., Clark, J.L., Koulen, P., Kaja, S., 2012. Plate reader-based assays for measuring cell viability, neuroprotection and calcium in primary neuronal cultures. J. Neurosci. Methods 203, 141–145.
Calkins, D.J., 2012. Critical pathogenic events underlying progression of neurodegeneration in glaucoma. Prog. Retin. Eye Res. 31, 702–719.
Cooper, M.L., Collyer, J.W., Calkins, D.J., 2018. Astrocyte remodeling without gliosis precedes optic nerve Axonopathy. Acta Neuropathol Commun 6, 38.
Crawford Downs, J., Roberts, M.D., Sigal, I.A., 2011. Glaucomatous cupping of the lamina cribrosa: a review of the evidence for active progressive remodeling as a mechanism. Exp. Eye Res. 93, 133–140.
Fan Gaskin, J.C., Shah, M.H., Chan, E.C., 2021. Oxidative stress and the role of NADPH oxidase in glaucoma. Antioxidants 10, 238.
Fuchshofer, R., 2011. The pathogenic role of transforming growth factor-β2 in glaucomatous damage to the optic nerve head. Exp. Eye Res. 93, 165–169.
Fuchshofer, R., Tamm, E.R., 2012. The role of TGF-β in the pathogenesis of primary open-angle glaucoma. Cell Tissue Res. 347, 279–290.
Ghosh, A.K., Cesna, R., Neverauskas, D., Ziniauskaite, A., Iqbal, S., Eby, J.M., Ragauskas, S., Kaja, S., 2023. Dietary Alcohol consumption elicits corneal toxicity through the generation of cellular oxidative stress. J Ocul Pharmacol Ther 39, 303–316.
Ghosh, A.K., Rao, V.R., Wisniewski, V.J., Zigrossi, A.D., Floss, J., Koulen, P., Stubbs Jr., E.B., Kaja, S., 2020. Differential activation of glioprotective intracellular signaling pathways in primary optic nerve head astrocytes after treatment with different classes of antioxidants. Antioxidants 9, 324.
Gurung, S., Perocheau, D., Touramanidou, L., Baruteau, J., 2021. The exosome journey: from biogenesis to uptake and intracellular signalling. Cell Commun. Signal. 19, 47.
Harwerth, R.S., Quigley, H.A., 2006. Visual field defects and retinal ganglion cell losses in patients with glaucoma. Arch. Ophthalmol. 124, 853–859.
Hernandez, M.R., 2000. The optic nerve head in glaucoma: role of astrocytes in tissue remodeling. Prog. Retin. Eye Res. 19, 297–321.
Hernandez, M.R., Agapova, O.A., Yang, P., Salvador-Silva, M., Ricard, C.S., Aoi, S., 2002. Differential gene expression in astrocytes from human normal and glaucomatous optic nerve head analyzed by cDNA microarray. Glia 38, 45–64.
Kaja, S., Payne, A.J., Naumchuk, Y., Koulen, P., 2017. Quantification of lactate dehydrogenase for cell viability testing using cell lines and primary cultured astrocytes. Curr Protoc Toxicol 72, 2.26.1-2.26.10.
Kaja, S., Payne, A.J., Naumchuk, Y., Levy, D., Zaidi, D.H., Altman, A.M., Nawazish, S., Ghuman, J.K., Gerdes, B.C., Moore, M.A., Koulen, P., 2015a. Plate reader-based cell viability assays for glioprotection using primary rat optic nerve head astrocytes. Exp. Eye Res. 138, 159–166.
Kaja, S., Payne, A.J., Patel, K.R., Naumchuk, Y., Koulen, P., 2015b. Differential subcellular Ca2+ signaling in a highly specialized subpopulation of astrocytes. Exp. Neurol. 265, 59–68.
Kaja, S., Stubbs, E.B., Mitchell, C.H., Ghosh, A.K., 2020. Mechanical strain results causes cytoskeletal remodeling and cellular elastinopathy in primary optic nerve head astrocytes. Investigative Ophthalmology & Visual Science 61,, 992.
Kalra, H., Simpson, R.J., Ji, H., Aikawa, E., Altevogt, P., Askenase, P., Bond, V.C., Borras, F.E., Breakefield, X., Budnik, V., Buzas, E., Camussi, G., Clayton, A., Cocucci, E., Falcon-Perez, J.M., Gabrielsson, S., Gho, Y.S., Gupta, D., Harsha, H.C., Hendrix, A., Hill, A.F., Inal, J.M., Jenster, G., Kramer-Albers, E.M., Lim, S.K., Llorente, A., Lotvall, J., Marcilla, A., Mincheva-Nilsson, L., Nazarenko, I., Nieuwland, R., Nolte-'t Hoen, E.N., Pandey, A., Patel, T., Piper, M.G., Pluchino, S., Prasad, T.S., Rajendran, L., Raposo, G., Record, M., Reid, G.E., Sanchez-Madrid, F., Schiffelers, R.M., Siljander, P., Stensballe, A., Stoorvogel, W., Taylor, D., Thery, C., Valadi, H., van Balkom, B.W., Vazquez, J., Vidal, M., Wauben, M.H., Yanez-Mo, M., Zoeller, M., Mathivanan, S., 2012. Vesiclepedia: a compendium for extracellular vesicles with continuous community annotation. PLoS Biol. 10, e1001450.
Kapetanakis, V.V., Chan, M.P., Foster, P.J., Cook, D.G., Owen, C.G., Rudnicka, A.R., 2016. Global variations and time trends in the prevalence of primary open angle glaucoma (POAG): a systematic review and meta-analysis. Br. J. Ophthalmol. 100, 86–93.
Karampoga, A., Tzaferi, K., Koutsakis, C., Kyriakopoulou, K., Karamanos, N.K., 2022. Exosomes and the extracellular matrix: a dynamic interplay in cancer progression. Int. J. Dev. Biol. 66, 97–102.
Kim, K.K., Sheppard, D., Chapman, H.A., 2018. TGF-β1 signaling and tissue fibrosis. Cold Spring Harbor Perspect. Biol. 10, a022293.
Kutchuk, L., Laitala, A., Soueid-Bomgarten, S., Shentzer, P., Rosendahl, A.H., Eilot, S., Grossman, M., Sagi, I., Sormunen, R., Myllyharju, J., Mäki, J.M., Hasson, P., 2015. Muscle composition is regulated by a Lox-TGFβ feedback loop. Development 142, 983–993.
Li, X., He, J., Sun, J., 2021. LOXL1 gene polymorphisms are associated with exfoliation syndrome/exfoliation glaucoma risk: an updated meta-analysis. PLoS One 16, e0250772.
Li, Z., Peng, F., Liu, Z., Li, S., Li, L., Qian, X., 2022. Mechanobiological responses of astrocytes in optic nerve head due to biaxial stretch. BMC Ophthalmol. 22, 368.
Liu, B., Neufeld, A.H., 2000. Expression of nitric oxide synthase-2 (NOS-2) in reactive astrocytes of the human glaucomatous optic nerve head. Glia 30, 178–186.
Liu, C., Zhu, P., Wang, W., Li, W., Shu, Q., Chen, Z.J., Myatt, L., Sun, K., 2016. Inhibition of lysyl oxidase by prostaglandin E2 via EP2/EP4 receptors in human amnion fibroblasts: implications for parturition. Mol. Cell. Endocrinol. 424, 118–127.
Liu, J., Jiang, F., Jiang, Y., Wang, Y., Li, Z., Shi, X., Zhu, Y., Wang, H., Zhang, Z., 2020. Roles of exosomes in ocular diseases. Int. J. Nanomed. 15, 10519–10538.
Liu, Y.X., Sun, H., Guo, W.Y., 2022. Astrocyte polarization in glaucoma: a new opportunity. Neural Regen Res 17, 2582–2588.
Livak, K.J., Schmittgen, T.D., 2001. Analysis of relative gene expression data using real-time quantitative PCR and the 2(-Delta Delta C(T)) Method. Methods 25, 402–408.
Lowry, O.H., Rosebrough, N.J., Farr, A.L., Randall, R.J., 1951. Protein measurement with the Folin phenol reagent. J. Biol. Chem. 193, 265–275.
Lu, W., Albalawi, F., Beckel, J.M., Lim, J.C., Laties, A.M., Mitchell, C.H., 2017. The P2X7 receptor links mechanical strain to cytokine IL-6 up-regulation and release in neurons and astrocytes. J. Neurochem. 141, 436–448.
Luther, K.M., Haar, L., McGuinness, M., Wang, Y., Lynch Iv, T.L., Phan, A., Song, Y., Shen, Z., Gardner, G., Kuffel, G., Ren, X., Zilliox, M.J., Jones, W.K., 2018. Exosomal miR-21a-5p mediates cardioprotection by mesenchymal stem cells. J. Mol. Cell. Cardiol. 119, 125–137.
Mashouri, L., Yousefi, H., Aref, A.R., Ahadi, A.M., Molaei, F., Alahari, S.K., 2019. Exosomes: composition, biogenesis, and mechanisms in cancer metastasis and drug resistance. Mol. Cancer 18, 75.
Mead, B., Ahmed, Z., Tomarev, S., 2018. Mesenchymal stem cell-derived small extracellular vesicles promote neuroprotection in a genetic DBA/2J mouse model of glaucoma. Invest. Ophthalmol. Vis. Sci. 59, 5473–5480.
Mead, B., Tomarev, S., 2017. Bone marrow-derived mesenchymal stem cells-derived exosomes promote survival of retinal ganglion cells through miRNA-dependent mechanisms. Stem Cells Transl Med 6, 1273–1285.
Meijering, E., Jacob, M., Sarria, J.C., Steiner, P., Hirling, H., Unser, M., 2004. Design and validation of a tool for neurite tracing and analysis in fluorescence microscopy images. Cytometry 58, 167–176.
Naumann, G.O., Schlotzer-Schrehardt, U., Kuchle, M., 1998. Pseudoexfoliation syndrome for the comprehensive ophthalmologist. Intraocular and systemic manifestations. Ophthalmology 105, 951–968.

Navneet, S., Rohrer, B., 2022. Elastin turnover in ocular diseases: a special focus on age-related macular degeneration. Exp. Eye Res. 222, 109164.
Pappenhagen, N., Yin, E., Morgan, A.B., Kiehlbauch, C.C., Inman, D.M., 2022. Stretch stress propels glutamine dependency and glycolysis in optic nerve head astrocytes. Front. Neurosci. 16, 957034.
Pekny, M., Pekna, M., 2014. Astrocyte reactivity and reactive astrogliosis: costs and benefits. Physiol. Rev. 94, 1077–1098.
Pena, J.D., Netland, P.A., Vidal, I., Dorr, D.A., Rasky, A., Hernandez, M.R., 1998. Elastosis of the lamina cribrosa in glaucomatous optic neuropathy. Exp. Eye Res. 67, 517–524.
Plateroti, P., Plateroti, A.M., Abdolrahimzadeh, S., Scuderi, G., 2015. Pseudoexfoliation syndrome and pseudoexfoliation glaucoma: a review of the literature with updates on surgical management. J Ophthalmol 2015, 370371.
Quigley, E.N., Quigley, H.A., Pease, M.E., Kerrigan, L.A., 1996. Quantitative studies of elastin in the optic nerve heads of persons with primary open-angle glaucoma. Ophthalmology 103, 1680–1685.
Quigley, H.A., Addicks, E.M., Green, W.R., Maumenee, A.E., 1981. Optic nerve damage in human glaucoma. II. The site of injury and susceptibility to damage. Arch. Ophthalmol. 99, 635–649.
Quigley, H.A., Brown, A., Dorman-Pease, M.E., 1991. Alterations in elastin of the optic nerve head in human and experimental glaucoma. Br. J. Ophthalmol. 75, 552–557.
Quigley, H.A., Green, W.R., 1979. The histology of human glaucoma cupping and optic nerve damage: clinicopathologic correlation in 21 eyes. Ophthalmology 86, 1803–1830.
Roy, R., Polgar, P., Wang, Y., Goldstein, R.H., Taylor, L., Kagan, H.M., 1996. Regulation of lysyl oxidase and cyclooxygenase expression in human lung fibroblasts: interactions among TGF-beta, IL-1 beta, and prostaglandin E. J. Cell. Biochem. 62, 411–417.
Schlotzer-Schrehardt, U., Hammer, C.M., Krysta, A.W., Hofmann-Rummelt, C., Pasutto, F., Sasaki, T., Kruse, F.E., Zenkel, M., 2012. LOXL1 deficiency in the lamina cribrosa as candidate susceptibility factor for a pseudoexfoliation-specific risk of glaucoma. Ophthalmology 119, 1832–1843.
Schlotzer-Schrehardt, U., Zenkel, M., 2019. The role of lysyl oxidase-like 1 (LOXL1) in exfoliation syndrome and glaucoma. Exp. Eye Res. 189, 107818.
Sethi, A., Mao, W., Wordinger, R.J., Clark, A.F., 2011. Transforming growth factor–β induces extracellular matrix protein cross-linking lysyl oxidase (LOX) genes in human trabecular meshwork cells. Investigative ophthalmology & visual science 52, 5240–5250.
Sharif, N.A., 2018. Glaucomatous optic neuropathy treatment options: the promise of novel therapeutics, techniques and tools to help preserve vision. Neural Regen Res 13, 1145–1150.
Shi, H., Wang, M., Sun, Y., Yang, D., Xu, W., Qian, H., 2021. Exosomes: emerging cell-free based therapeutics in dermatologic diseases. Front. Cell Dev. Biol. 9, 736022.
Shim, M.S., Kim, K.Y., Bu, J.H., Nam, H.S., Jeong, S.W., Park, T.L., Ellisman, M.H., Weinreb, R.N., Ju, W.K., 2018. Elevated intracellular cAMP exacerbates vulnerability to oxidative stress in optic nerve head astrocytes. Cell Death Dis. 9, 285.
Sicot, F.X., Tsuda, T., Markova, D., Klement, J.F., Arita, M., Zhang, R.Z., Pan, T.C., Mecham, R.P., Birk, D.E., Chu, M.L., 2008. Fibulin-2 is dispensable for mouse development and elastic fiber formation. Mol. Cell Biol. 28, 1061–1067.
Soles, A., Selimovic, A., Sbrocco, K., Ghannoum, F., Hamel, K., Moncada, E.L., Gilliat, S., Cvetanovic, M., 2023. Extracellular matrix regulation in physiology and in brain disease. Int. J. Mol. Sci. 24.
Sun, D., Moore, S., Jakobs, T.C., 2017. Optic nerve astrocyte reactivity protects function in experimental glaucoma and other nerve injuries. J. Exp. Med. 214, 1411–1430.
Tehrani, S., Davis, L., Cepurna, W.O., Delf, R.K., Lozano, D.C., Choe, T.E., Johnson, E.C., Morrison, J.C., 2019. Optic nerve head astrocytes display axon-dependent and -independent reactivity in response to acutely elevated intraocular pressure. Invest. Ophthalmol. Vis. Sci. 60, 312–321.
Thakur, A., Shah, D., Rai, D., Parra, D.C., Pathikonda, S., Kurilova, S., Cili, A., 2023. Therapeutic values of exosomes in cosmetics, skin care, tissue regeneration, and dermatological diseases. Cosmetics 10, 65.
Thery, C., Amigorena, S., Raposo, G., Clayton, A., 2006. Isolation and characterization of exosomes from cell culture supernatants and biological fluids. Curr Protoc Cell Biol Chapter 3. Unit 3 22.
Thery, C., Ostrowski, M., Segura, E., 2009. Membrane vesicles as conveyors of immune responses. Nat. Rev. Immunol. 9, 581–593.
van Niel, G., D'Angelo, G., Raposo, G., 2018. Shedding light on the cell biology of extracellular vesicles. Nat. Rev. Mol. Cell Biol. 19, 213–228.
Varela, H.J., Hernandez, M.R., 1997. Astrocyte responses in human optic nerve head with primary open-angle glaucoma. J. Glaucoma 6, 303–313.
Wallace, D.M., O'Brien, C.J., 2016. The role of lamina cribrosa cells in optic nerve head fibrosis in glaucoma. Exp. Eye Res. 142, 102–109.
Wang, R., Seifert, P., Jakobs, T.C., 2017. Astrocytes in the optic nerve head of glaucomatous mice display a characteristic reactive phenotype. Invest. Ophthalmol. Vis. Sci. 58, 924–932.
Weinreb, R.N., Aung, T., Medeiros, F.A., 2014. The pathophysiology and treatment of glaucoma: a review. JAMA 311, 1901–1911.
Weinreb, R.N., Leung, C.K., Crowston, J.G., Medeiros, F.A., Friedman, D.S., Wiggs, J.L., Martin, K.R., 2016. Primary open-angle glaucoma. Nat. Rev. Dis. Prim. 2, 16067.
Wu, K.Y., Ahmad, H., Lin, G., Carbonneau, M., Tran, S.D., 2023. Mesenchymal stem cell-derived exosomes in Ophthalmology: a comprehensive review. Pharmaceutics 15, 1167.
Yokoyama, U., Minamisawa, S., Shioda, A., Ishiwata, R., Jin, M.-H., Masuda, M., Asou, T., Sugimoto, Y., Aoki, H., Nakamura, T., Ishikawa, Y., 2014. Prostaglandin E_2 inhibits elastogenesis in the ductus arteriosus via EP4 signaling. Circulation 129, 487–496.
Yuksel, N., Yilmaz Tugan, B., 2023. Pseudoexfoliation glaucoma: clinical presentation and therapeutic options. Turk J Ophthalmol 53, 247–256.
Zhang, W., Hong, J., Zhang, H., Zheng, W., Yang, Y., 2021. Astrocyte-derived exosomes protect hippocampal neurons after traumatic brain injury by suppressing mitochondrial oxidative stress and apoptosis. Aging (Albany NY) 13, 21642–21658.
Zhang, Y., Liu, Y., Liu, H., Tang, W.H., 2019. Exosomes: biogenesis, biologic function and clinical potential. Cell Biosci. 9, 19.
Zhao, S., Sheng, S., Wang, Y., Ding, L., Xu, X., Xia, X., Zheng, J.C., 2021. Astrocyte-derived extracellular vesicles: a double-edged sword in central nervous system disorders. Neurosci. Biobehav. Rev. 125, 148–159.
Zhu, Y., Wang, R., Pappas, A.C., Seifert, P., Savol, A., Sadreyev, R.I., Sun, D., Jakobs, T. C., 2023. Astrocytes in the optic nerve are heterogeneous in their reactivity to glaucomatous injury. Cells 12, 2131.